https://doi.org/10.5194/egusphere-2026-4640
Preprint. Discussion started: 20 November 2026
© Author(s) 2026. CC BY 4.0 License.

Extension of a Ground-Based Tropospheric Remote Sensing Methodology to the Marine Atmospheric Surface Layer

Caleb R. Sease[1], Daniel P. Greenway[1], Andrew J. Kammerer[2], David D. Flagg[3] and, Erin E. Hackett[1]

[1]Department of Marine Science, Coastal Carolina University, Conway, SC, 29576, USA
[2]DeVine Consulting, Inc. Fremont, CA, 94538, USA
[3]U.S. Naval Research Laboratory, Monterey, CA, 93943, USA

Correspondence to: Erin E. Hackett (ehackett@coastal.edu)

Abstract. Increasing the fidelity and coverage of marine atmospheric surface layer (MASL) thermodynamic measurements is beneficial; for example, providing data for assimilation into numerical weather prediction (NWP) models, long term climate analysis, improving surface layer model parameterizations, and improving the accuracy of radio frequency (RF) propagation models. However, modern methods of measuring or modelling thermodynamic profiles in the MASL are limited by accuracy, spatial coverage, vertical resolution, computational efficiency, and/or temporal resolution. Many ground-based remote sensing technologies have been developed to estimate thermodynamic properties, but typically do not extend into the surface layer. They commonly utilize remote sensing data acquired at altitudes above 150 m and at relatively coarse resolution (> 100 m). In the last two decades, ground-based radar has been utilized to develop refractivity remote sensing techniques in the MASL, which can provide fine-scale vertical distributions of refractivity at altitudes below 100 m. To these ends, the authors investigate how these higher altitude methods can be merged with these recent advancements in refractivity remote sensing in the MASL. We find that tropospheric thermodynamic remote sensing techniques can be extended into the MASL to accurately retrieve humidity from estimates of surface layer temperature and refractivity; thus, remote sensing of high resolution MASL humidity may be possible.

1 Introduction

Measurements of moisture vertical profiles in the surface layer of the atmosphere are relevant to numerous scientific areas of study as well as many engineering applications. Assimilation of accurate thermodynamic surface layer profiles into weather models can greatly improve accuracy of forecasts (Ruggiero et al., 1995; Otkin et al., 2011), which on longer timescales influence climate predictions. These models rely on parameterizations of surface layer processes that would be better guided by less expensive and more abundant surface layer measurements. Moreover, surface layer thermodynamic variables are necessary for accurate prediction of communication and sensor performance in the marine atmospheric surface layer (MASL). The MASL is a challenging region of the air column to measure and model due to the large

https://doi.org/10.5194/egusphere-2026-4640
Preprint. Discussion started: 20 November 2026
© Author(s) 2026. CC BY 4.0 License.

gradients of moisture near the surface as well as the turbulent and convective nature of flow in this region (Edson and Fairall, 1998). *In-situ* radiosonde measurements are typically used as a ground truth in many atmospheric studies as they provide accurate estimates of thermodynamic variables, however, they are unable to cover large spatial scales simultaneously, capture instantaneous vertical profiles without specialized measuring platforms (Stanek et al., 2023), or resolve the surface layer well without contamination from the launching platform (Kang and Wang, 2016); not to mention the high financial cost of such labour-intensive measurements over water. In contrast, numerical weather prediction (NWP) is frequently employed due to its vast spatial and temporal coverage, but numerical models lack fidelity at small scales that are important in the MASL (Calaf et al., 2023) such as, estimating thermodynamic variables at relatively low vertical resolution for MASL processes; not to mention the computational expense of such simulations. Monin-Obukhov similarity theory (MOST) algorithms are often employed in the MASL to generate surface layer vertical profiles using measurements of thermodynamic and wind variables at only two reference points, which can be blended with NWP forecasts. It is also well known that MOST has limitations especially in stable atmospheres over water (Wang et al., 2024) and over wavy surfaces (Stanek, 2023).

These shortcomings make remote sensing of thermodynamic variables in the atmosphere attractive. Modern remote sensing methods often require a combination of passive and active sensors to retrieve vertical profiles of moisture and temperature (Bianco et al., 2024; Che et al., 2019). Gossard et al. (1995) used ground-based Doppler wind profiling radars (WPR) to retrieve vertical gradients of potential refractivity. They further proposed that this refractivity retrieval technique, in conjunction with a Radio Acoustic Sounding System (RASS) to retrieve vertical profiles of potential temperature, could retrieve vertical profiles of the specific humidity gradient ($\mathrm{g\ kg^{-1}\ m^{-1}}$) using:

$$\frac{dq}{dz} = {b_g}^{-1}\left(\frac{d\phi}{dz} + a_g \frac{d\theta}{dz}\right) \tag{1}$$

where ϕ is potential atmospheric refractivity (N-units), θ is potential temperature (K), z is altitude (m), and:

$$\text{-}a_g = -\frac{77{,}600}{\theta^2} - \frac{1{,}199{,}696q}{\theta^3} \tag{2}$$

$$b_g = \frac{599{,}848}{\theta^2} \tag{3}$$

a_g and b_g were shown to be approximately constant in a near-standard atmosphere with $a_g \cong 1\ (\mathrm{K^{-1}})$ and $b_g \cong 7\ (\mathrm{kg\ g^{-1}})$.

Stankov et al. (2003) showed viability of the Gossard et al., (1995) proposed technique by retrieving humidity gradients using WPR-inverted potential refractivity gradients along with radiosonde-measured temperature gradients. These retrieved moisture profiles were in good agreement with radiosonde moisture profiles. This technique requires the use of

https://doi.org/10.5194/egusphere-2026-4640
Preprint. Discussion started: 20 November 2026
© Author(s) 2026. CC BY 4.0 License.

two remote sensing platforms, both WPR and RASS (with radiosonde temperature used as a proxy for RASS in the Stankov et al. (2003) study), and is limited to a relatively coarse vertical spacing of 100m. Thus, it does not retrieve humidity vertical profiles within the surface layer.

While WPR inversions may be limited to estimates outside of the surface layer due to its coarse vertical resolution, many studies have shown that refractivity can be accurately inverted for using point-to-point radio wave propagation measurements or sea clutter in the MASL (Pastore et al., 2022; Karimian et al., 2011, 2012, 2013; Yardim et al., 2006, 2008, 2009; Gerstoft et al., 2001, 2003; Rogers et al., 2000, 2005; Matsko and Hackett, 2019; Penton and Hackett, 2018; Zhao et al., 2011, 2017), and in some cases can even be used to retrieve spatially heterogeneous refractive environments (Greenway et al., 2024, 2025). These inversion techniques estimate model parameters that can be used to estimate vertical profiles of atmospheric refractivity in the MASL. Therefore, to obtain instantaneous vertical profiles of specific humidity gradients in the MASL, the methodology outlined by Gossard et al. (1995) and examined in Stankov et al. (2003), could be extended to the MASL using an estimate of refractivity from a ground-based radar plus an estimate of temperature from NWP or another ground based sensor. NWP has been shown to more accurate predict temperature when compared to NWP moisture estimates in the MASL (Sease et al., 2024). Thus, accurate retrievals of vertical moisture profiles may be possible with the combination of MASL refractivity retrievals and NWP temperature profiles. However, the coefficients (a_g and b_g) used in Gossard et al. (1995) were approximate and intended for altitudes primarily above the MASL, thus further investigation into the applicability of those coefficients in the MASL is needed.

Refractivity from sea clutter and point-to-point propagation inversions are not in potential form. Moreover, hydrostatic pressure in the MASL typically decreases linearly with altitude, thus, direct extension of Eq. (1) to the MASL may not be necessary. As such, in this manuscript, we modify Eq. (1) for extension into the MASL and for use in connection with refractivity retrievals (i.e., a non-potential form of Eq. [1]) and examine the variability of the coefficients in this modified Eq. (1) in order to evaluate the applicability of the Gossard et al. (1995) methodology in the MASL. For example, the assumption of constant coefficients may not be valid in the MASL due to the presence of large vertical thermodynamic and momentum gradients. These insights help determine feasibility of estimating humidity gradient vertical profiles in the MASL based on measurement of temperature and X-band radar-based refractivity; enabling remote sensing of moisture in the MASL.

2 Refractive Gradients

Eq. (1) (Gossard et al., 1995) can be modified to non-potential form, which could be suitable for use with radar-based MASL refractivity and hence extension into the MASL. The Bean and Dutton (1966) formulation of atmospheric refractivity, with a conversion to specific humidity is (Gossard et al., 1995):

https://doi.org/10.5194/egusphere-2026-4640
Preprint. Discussion started: 20 November 2026
© Author(s) 2026. CC BY 4.0 License.

$$N = \frac{77.6}{T} p \left(1 + \frac{7.73\, q}{T}\right) \quad (4)$$

where N is atmospheric refractivity (N-units), p is pressure (mbar), T is temperature (K), and q is specific humidity (g kg^{-1}). The derivative of Eq. (4) with respect to altitude, and rearranging to solve for humidity vertical gradients, is:

$$\frac{dq}{dz} = b^{-1} \left(\frac{dN}{dz} + a \frac{dT}{dz} - c \frac{dp}{dz}\right) \quad (5)$$

with

$$-a = -\frac{77.6\mathrm{p}}{\mathrm{T}^2} \left(1 + 15.46 \frac{q}{T}\right) \quad (6)$$

$$b = \left(\frac{599.848p}{T^2}\right) \quad (7)$$

$$c = \frac{77.6}{T} \left(1 + 7.73 \frac{q}{T}\right) \quad (8)$$

Eq. (5) is very similar to its potential counterpart (Eq. [1]); the main difference being there is a pressure gradient term along with a new coefficient that we denote as c (Eq. [8]); in fact this form of the equation was derived by Bean and Dutton (1966) without the specific humidity conversion. Hereafter, when referring to the set of coefficients (*a, b,* and *c*), we will use the variable Ω.

3 Coefficient Evaluation Data

To evaluate the coefficients in Eq. (5-8), we use a wide variety of data with various sources. Specifically, we use NWP and *in-situ* data as they are co-located and synchronous in time, providing an exact ground truth, which is not possible using radar-based refractivity retrievals. Furthermore, this vast dataset allows for the evaluation of these coefficients during different atmospheric conditions and may provide insights into the validity of assuming constant coefficients in the MASL over a statistically significant sample size. Different sources of data (e.g., weather forecasts vs. *in-situ* measurements) are also used to ensure the coefficient analysis isn't biased toward a particular data source.

https://doi.org/10.5194/egusphere-2026-4640
Preprint. Discussion started: 20 November 2026
© Author(s) 2026. CC BY 4.0 License.

3.1 Field Campaigns

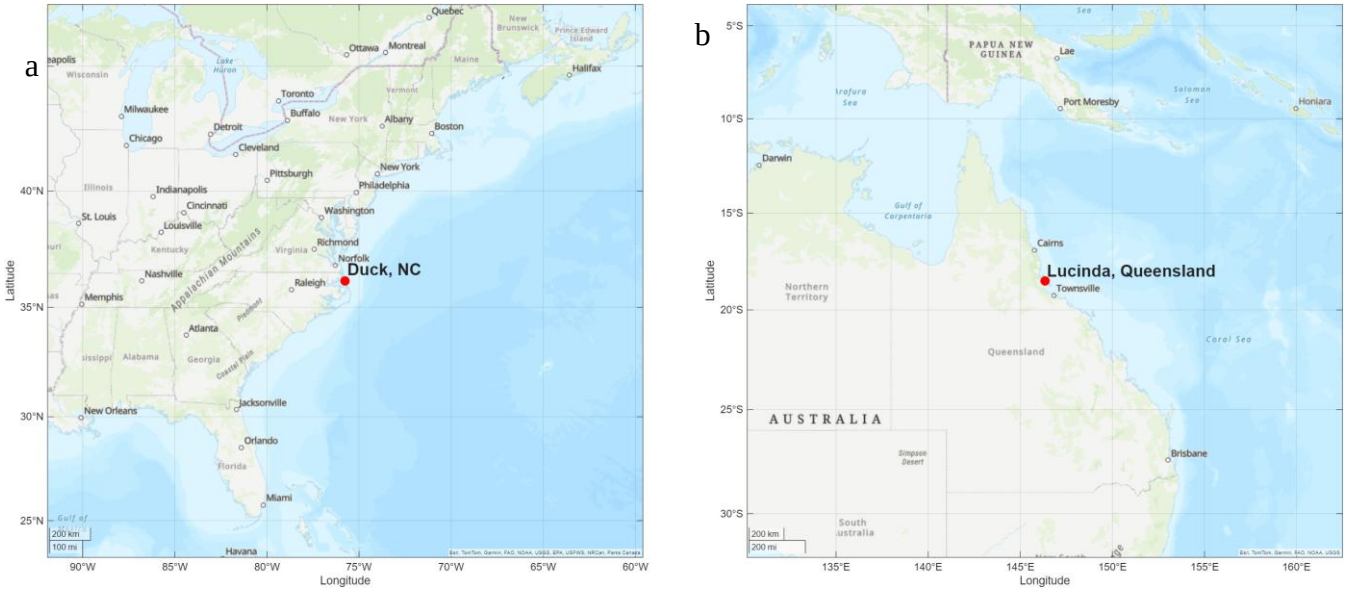


Figure 1: Locations of each field campaign: CASPER-East (a) and TAPS (b). Sources: Esri, TomTom, Garmin, FAO, NOAA, USGS, EPA, USFWS, NRCan, Parks Canada | Powered by Esri.

3.1.1 CASPER-East Field Campaign

The Coupled Air Sea Processes and Electromagnetic Ducting Research – East field campaign (CASPER-East) was conducted off the coast of Duck, North Carolina from October 10 to November 6, 2015 (Wang et al., 2018), as shown in fig. 1a. This campaign's goal was to obtain electromagnetic wave propagation measurements across a range of different meteorological conditions with a particular focus on ducting conditions. Data were collected primarily along an offshore transect from Duck pier to the Gulf Stream yielding large variability in sea surface temperatures (SST). Bulk *in-situ* measurements taken from a bow mast on one of the research vessels, the R/V Hugh R. Sharp, shows specific humidity variations ranging from approximately 5 to 15 g kg^{-1} with a mean specific humidity over the entire time period of approximately 7 g kg^{-1}. Similarly, (approximately) sea level pressure and temperature had variations ranging from 1000 to 1025 hPa and 283 to 293 K, respectively (Wessinger et al., 2024). There were also a couple fronts that moved through the region during the field campaign (Wang et al., 2018).

3.1.2 TAPS Field Campaign

To diversify atmospheric conditions, we also utilize data associated with the Tropical Air-Sea Propagation Study (TAPS) field campaign, which was conducted off the coast of north-eastern Australia from November 24 to December 5, 2013

https://doi.org/10.5194/egusphere-2026-4640
Preprint. Discussion started: 20 November 2026
© Author(s) 2026. CC BY 4.0 License.

(Kulessa et al., 2017) (Fig. 1b). The TAPS dataset provides atmospheric conditions that were unseen during the CASPER-East field campaign, allowing for the analysis of these methodologies in a low latitude, high humidity environment (Kammerer et al., 2018). Average temperature, humidity, and sea level pressure, computed from all TAPS *in-situ* and numerical datasets, were roughly 299K, 13 g kg^{-1}, and 1008 hPa, respectively (Kulessa et al., 2017). These mean humidity and temperature estimates reveal how much warmer and wetter the environment during the TAPS experiment was on-average when compared to the CASPER-East averages. Also, unlike CASPER-East, and due to the low latitude of the TAPS campaign, frontogenesis is uncommon and was not observed during this campaign.

3.2 COAMPS® Forecasts

The Coupled Ocean/Atmosphere Mesoscale Prediction System (COAMPS®; Hodur 1997) was used to produce forecasts for each field campaign. Every forecast contains instantaneous vertical profiles of each thermodynamic variable involved in Eq. (4) and (5). The COAMPS model does not provide fine enough vertical resolution to resolve details within the surface layer; thus, the Navy Atmospheric Vertical Surface Layer Model (NAVSLaM; Frederickson, 2015) is blended with the COAMPS forecast to create vertical profiles with decimeter resolution in the first 100 meters of the atmosphere (COAMPS-NAVSLaM blended vertical profiles will henceforth be referred to as COAMPS).

It is important to note that the CASPER-East COAMPS (henceforth referred to as CE-NWP) forecasts were verified against *in-situ* data and numerous recent studies have utilized this NWP data, especially for the prediction of refractive environments (Xu et al., 2022; Ulate et al., 2019; Pastore et al., 2021; Pastore et al., 2023; Wessinger et al., 2024; Greenway et al., 2024). In addition, the density of data in terms of spatial and temporal coverage make it more ideal to use than *in-situ* data. The CASPER-East numerical dataset contains 648 hourly forecasts at 31 different ranges along the offshore transect (20,088 vertical profiles). Specifically, these forecasts extend from Duck Pier, North Carolina, to approximately 61.32 km offshore.

The TAPS COAMPS data (henceforth referred to as TAPS-NWP), which was also verified with *in-situ* data (Kulessa et al., 2017), includes 264 COAMPS hourly forecasts at 52 different ranges (13,728 vertical profiles). These forecasts extend from the northeastern shore of Australia, near the town of Lucinda, to approximately 86.72 km offshore.

3.3 *In-situ* Measurements

To ensure results aren't biased toward the NWP (and NAVSLaM) model, we also incorporate other data sources from CASPER-East. One high-fidelity set of *in-situ* measurements taken during CASPER-East were measured by the Marine Atmospheric Profiling System (MAPS) (Wang et al., 2018) (henceforth referred to as CE-MAPS). A small inflatable manned vessel was used as a platform for these measurements to ensure limited contamination of measurements by the larger research vessel; thus, these measurements are considered highly accurate (Pastore et al., 2023). These measurements were

https://doi.org/10.5194/egusphere-2026-4640
Preprint. Discussion started: 20 November 2026
© Author(s) 2026. CC BY 4.0 License.

taken via a radiosonde attached to a tethered weather balloon. In total, this dataset contains 302 vertical profiles of thermodynamic variables between ~0.5 m to ~60 m above sea level. Each profile contains one ascent and descent of the radiosonde attached to the weather balloon, each ascent and descent occur over approximately one minute. Evaluating the coefficients with these measurements provide a different type of data source in a similar environment (i.e., CASPER-East/Duck, NC), which will help evaluate any bias our results may have towards the COAMPS/NAVSLaM model. Because *in-situ* measurement coverage is comparatively sparse, we use the verified weather model data as the main data source to achieve high statistical significance of results while relying on *in-situ* data to provide confidence in those results.

4 Coefficient Analysis Methods

To examine the variability of the *a, b,* and *c* coefficients (Ω), we use two approaches. In the first approach, we use the formulas defined in Eq. (6-8) using the temperature, pressure, and specific humidity from all data sources outlined above. The coefficient values computed using Eq. (6-8) (at every altitude will be referred to as Ω_c (with the subscript c indicating calculated coefficients).

In a second approach, to partly verify Eq. (6-8) as well as gain insights into optimal coefficient values, we apply a non-linear least squares regression to Eq. (5) using known specific humidity, temperature, pressure, and atmospheric refractivity gradients for all datasets. This approach provides the optimal coefficients to balance Eq. (10), compared to the first approach, which relies on ill-defined mean quantities to solve Eq. (6-8). We apply an initial guess of $a \approx 1\ (\mathrm{K}^{-1})$, $b \approx 7\ (\mathrm{kg\ g}^{-1})$, and $c \approx 0.3\ (\mathrm{hPa}^{-1})$ to the non-linear fit, which is based off of average calculated coefficients (Ω_c) and prior values in the literature for the potential form of the equation (Eq. 1; Gossard et al., 1995; Stankov et al., 2003). The non-linear fit and calculations (Eq. [6-8]) are performed altitude-by-altitude, resulting in vertical profiles of the coefficients at the same vertical resolution as the thermodynamic variables for both *in-situ* and numerical data. The coefficients associated with the non-linear fit will be referred to as Ω_f (with the subscript f indicating the non-linear least squares fit coefficients). Furthermore, the gradients of the thermodynamic quantities are denoted as CE-NWP gradients for CASPER-East NWP, CE-MAPS gradients for CASPER-East *in-situ*, and CE-TAPS gradients for TAPS NWP.

To help evaluate the sensitivity of Eq. (5) to the coefficients, we compute the specific humidity gradients from the vertical profiles of Ω and the known temperature, atmospheric refractivity, and pressure gradients. These specific humidity gradients are computed using both Ω_c and the Ω_f vertical profiles. To evaluate the accuracy of Ω_f and Ω_c, these specific humidity gradient vertical profiles are compared with known specific humidity gradient vertical profiles via a root mean square error (RMSE):

https://doi.org/10.5194/egusphere-2026-4640
Preprint. Discussion started: 20 November 2026
© Author(s) 2026. CC BY 4.0 License.

$$\psi_g = \left[\frac{1}{N}\sum_{i=1}^{N}\left(\frac{dq}{dz_i} - \widetilde{\frac{dq}{dz_i}}\right)^2\right]^{1/2} \quad (9)$$

where N is the number of altitudes, $\frac{dq}{dz}$ is the ground truth specific humidity gradient, and $\widetilde{\frac{dq}{dz}}$ is the specific humidity gradient estimated using Eq. (5) with either the Ω_f or Ω_c coefficients.

4.1 Humidity and Temperature Vertical Profile Accuracy

To further evaluate the accuracy of humidity gradients estimated using Eq. (5) (based on known or estimated refractivity, temperature, and pressure gradients along with prescribed constant coefficients), we estimate the humidity vertical profile and evaluate its accuracy because it is a more familiar quantity than the humidity gradients. The humidity gradients are used to estimate the humidity vertical profile by applying a first order Taylor series expansion iteratively (i.e., finite difference integration)), at each altitude starting from a known surface point:

$$\tilde{q}(z_i) = \tilde{q}(z_{i-1}) + \widetilde{\frac{dq}{dz}}(z_{i-1})\Delta z \quad (10)$$

where *i* is an altitude index and $\Delta z = z_i - z_{i-1}$. It is important to note that a surface specific humidity, from the COAMPS humidity profile, is needed to initiate the iterative process (i.e., $\tilde{q}(z_{i-1})$ at $z_{i-1} = 0$ m).

To quantify the accuracy of the humidity vertical profile, RMSE between the estimated humidity vertical profile from Eq. (5) and Eq. (10) and the ground truth specific humidity vertical profile is calculated:

$$\psi = \left[\frac{1}{N}\sum_{i=1}^{N}(q - \tilde{q})^2\right]^{1/2} \quad (11)$$

where q is the ground truth specific humidity and $\tilde{q}$ is the specific humidity estimated using Eq. (10) from the known surface humidity and the $\widetilde{\frac{dq}{dz}}$ estimated from Eq. (5) using either the Ω_f or Ω_c coefficients.

5 Coefficients in the MASL

Persistent large vertical fluxes of momentum, moisture, and heat near the air-sea interface typically result in large humidity and temperature gradients near the surface (Monin and Obukhov, 1954). Due to these large surface gradients and other surface interactions, it is possible that the coefficients in Eq. (5) may vary with altitude much more so than higher in the atmosphere. For example, in numerical data, where the surface boundary conditions are skin SST and typically an

https://doi.org/10.5194/egusphere-2026-4640
Preprint. Discussion started: 20 November 2026
© Author(s) 2026. CC BY 4.0 License.

assumption of 98% relative humidity, the specific humidity and temperature can change by several g kg^{-1} and degrees, respectively, between the surface and ~10 cm above it (Pastore et al., 2021).

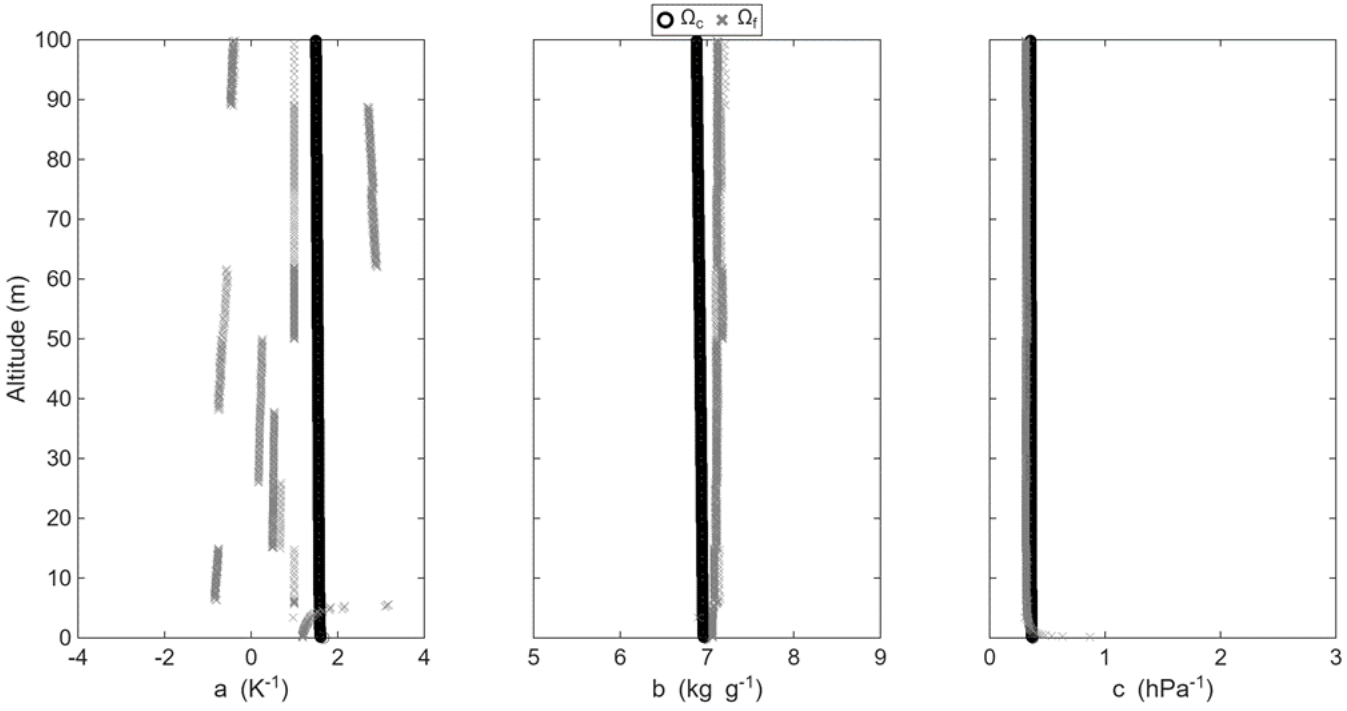


Figure 2. Example vertical profiles of all three coefficients estimated based on Eq. (6)-(8) (Ω_c) (black) and estimated with nonlinear least squares regression (Ω_f) (grey). Coefficients are computed from modelled thermodynamic profiles for a CASPER-East COAMPS forecast from 10/10/2015 01:00 UTC at 20.66 km offshore.

Results show limited vertical variability of the coefficients, Ω, as exemplified in fig. 2. Small vertical variability of Ω is consistent with the findings in Gossard et al. (1995) and Stankov et al. (2003) for the potential form of Eq. (5) (Eq. [1]). Especially the *b* and *c* coefficients have only minor variability with height, even at the surface. Furthermore, both the Ω_c and Ω_f are qualitatively in good agreement (Fig. 2). The variability of the non-linear fit *a* coefficient is due to an artifact of the non-linear fitting, and the more uniform vertical profile of the calculated *a* (Eq. [6]) is likely more accurate. The variability observed in the Ω_f occurs when the specific humidity gradient approaches zero (g $\mathrm{kg}^{-1}\mathrm{m}^{-1}$). In some cases, including the forecast shown in fig. 2, above 5 m in altitude, the humidity gradient is very small, and consequently, the fit *a* coefficient becomes less of a factor in balancing Eq. (5) causing instability in the optimization. In other words, Eq. (5) becomes insensitive to the *a* coefficient (in Ω_f) resulting in a relatively wide range of values balancing the equation. Because of this lack of sensitivity, coefficient values greater or less than 10 times $a \cong 1\ (\mathrm{K}^{-1}), b \cong 7\ (\mathrm{kg\,g}^{-1})$, and $c \cong 0.3\ (\mathrm{hPa}^{-1})$ are removed as outliers. Humidity gradients small enough to trigger this instability in the Ω_f are observed in ~35% of the vertical

https://doi.org/10.5194/egusphere-2026-4640
Preprint. Discussion started: 20 November 2026
© Author(s) 2026. CC BY 4.0 License.

profiles examined in this study; when the humidity gradient is sufficiently large, then the non-linear fit and calculated (Eq. [6]) *a* coefficients are similar and show little vertical variability like the *b* and *c* coefficients shown in fig. 2.

Fig. 3 shows the average coefficient, Ω, vertical profiles, where the average is taken over all the CE-NWP data. The Ω_c and Ω_f average vertical profiles are in relatively good agreement (Fig. 3), where $a \cong 1\ (\mathrm{K}^{-1})$, $b \cong 7\ (\mathrm{kg\,g}^{-1})$, and $c \cong 0.3\ (\mathrm{hPa}^{-1})$. Furthermore, there is very limited vertical variability of the coefficients on average, again suggesting that coefficients can likely be considered constants in the MASL similar to how a_g and b_g are set to fixed values when using Eq. (1) for detecting upper atmosphere humidity gradients (Gossard et al., 1995; Stankov et al., 2003). There is a small amount of variability in the values very near the surface (< 2 m), but the changes remain relatively small. Similar to the example in Fig. 2, the calculated (Eq. [7] and [8]) and non-linear fit *b* and *c* are in better agreement than the *a* coefficients.

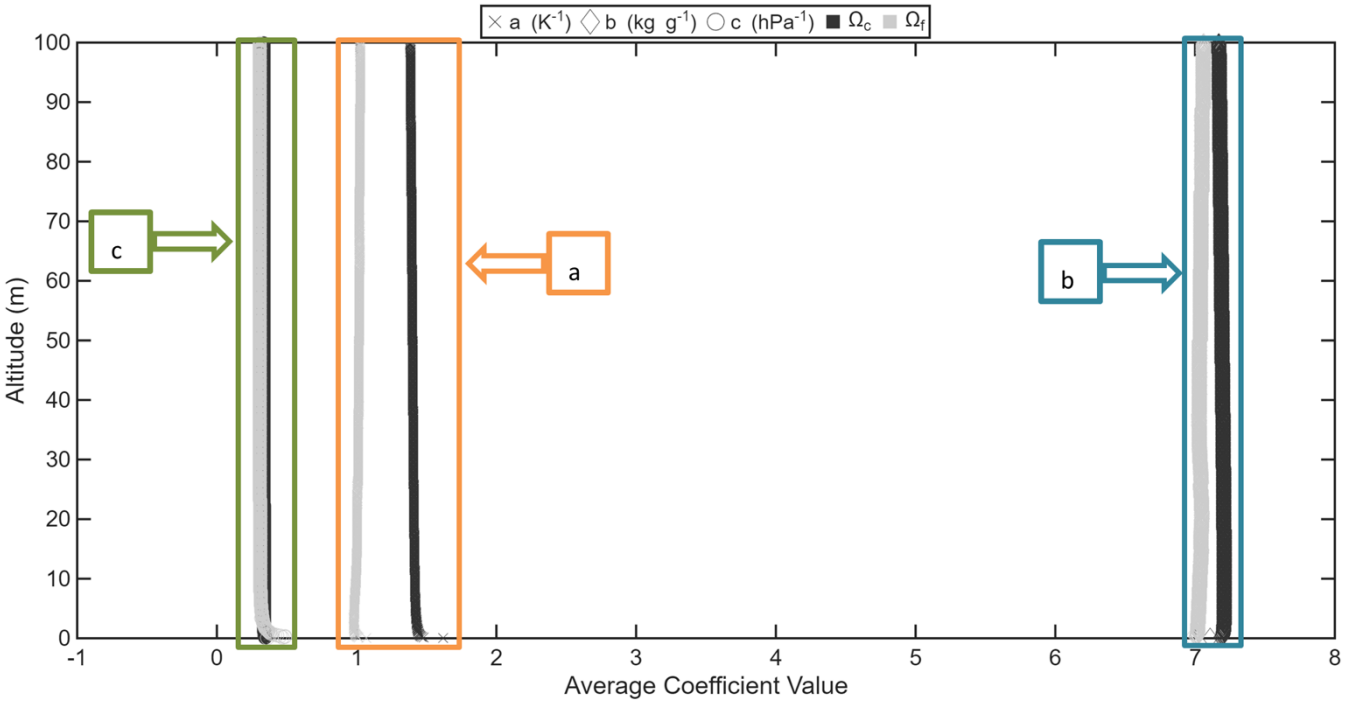


Figure 3. Mean coefficient vertical profiles for *a* (orange box), *b* (blue box), and *c* (green box) for Ω_c (Eq. [6-8], black) and Ω_f (Eq. [5], light grey) estimation methods (see legend). Averages are over all NWP CASPER-East forecasts including all ranges (a total of 20,088 thermodynamic profiles).

Using the coefficient vertical profiles estimated from the two methods (Ω_c and Ω_f), along with the temperature, refractivity, and pressure gradients of the NWP data, to compute specific humidity gradients via Eq. (5) results in very similar humidity gradients as the NWP data as shown in fig. 4, which shows a histogram of the RMSEs between the them (Ψ_g; Eq. [9]).

https://doi.org/10.5194/egusphere-2026-4640
Preprint. Discussion started: 20 November 2026
© Author(s) 2026. CC BY 4.0 License.

Ψ_g show very good agreement for Ω_f, as expected. This comparison is more-or-less a sanity check for the non-linear fitting as this agreement is dictated by the non-linear least squares regression, but it is useful to compare it against the humidity gradients computed using Ω_c. Use of the NWP data in Eq. (6-8) for estimating mean *T*, *p*, and *q* may lead to the differences between humidity gradients computed using Ω_f versus Ω_c. The time and/or spatial extent over which these quantities should be averaged prior to use in Eq. (6-8) is unclear and ill-defined. In comparison to Ω_f, the RMSEs of humidity gradients computed using Ω_c are more variable, and are, at times, large (Ψ_g > 0.1 g kg^{-1} m^{-1}) but are mostly on the order of 10^{-2}-10^{-4}, which is still several orders of magnitude higher than the linear fit Ψ_g, and can be on the order of magnitude of the gradient itself.

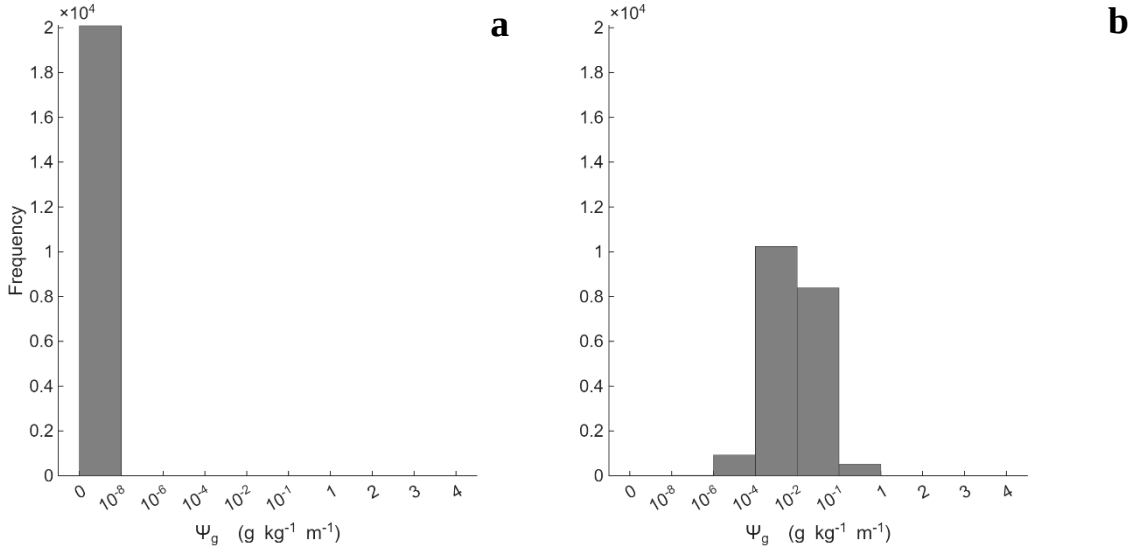


Figure 4. RMSE between estimated specific humidity gradients and the corresponding ground truth CE COAMPS specific humidity gradients (Ψ_g; Eq. [9]) when using the nonlinear least squares regression coefficients (Ω_f) (*a*) and coefficients estimated using Eq. (6)-(8) (Ω_c) (*b*).

Although results shown in this section were for the CE-NWP data, the other datasets (CE-MAPS and TAPS-NWP) showed similar results and are included in the statistical analysis discussed in the next section.

5.1 Statistical Coefficient Analysis

Table 1 shows average *a*, *b*, and *c* coefficients for both the calculation (Ω_c; Eq. [6-8]) and non-linear fit (Ω_f) estimation methods, where the average is taken over all altitudes, ranges, and instances for a given NWP or *in-situ* dataset. Prior to computing these averages, as previously stated, outlier coefficients that are plus or minus ten times a = 1.0 (K^{-1}), b = 7.0 ($\mathrm{kg\,g}^{-1}$), and c = 0.3 (hPa^{-1}) have been removed. Subsequently, coefficients greater or less than three standard deviations

https://doi.org/10.5194/egusphere-2026-4640
Preprint. Discussion started: 20 November 2026
© Author(s) 2026. CC BY 4.0 License.

from the mean coefficient are also removed. Recall the non-linear fitting can produce very large positive or negative coefficients as an artifact of balancing Eq. (1) when the humidity gradient is very small. Removing these values prior to computing the average coefficients shown in Table 1 prevents outliers from skewing the average values. The standard deviations show in Table 1 are also calculated after all these outliers have been removed.

Table 1. Average Ω_c and Ω_f plus and minus one standard deviation for NWP forecasts for the CASPER-East (CE-NWP) and TAPS (TAPS-NWP) field campaigns as well as from *in-situ* data from CASPER-East (CE-MAPS).

	Mean Ω_c			Mean Ω_f		
	a **(K^{-1})**	***b*** **($kg\ g^{-1}$)**	***c*** **(hPa^{-1})**	***a*** **(K^{-1})**	***b*** **($kg\ g^{-1}$)**	***c*** **(hPa^{-1})**
CE-NWP	1.4 ± 0.1	7.2 ± 0.2	0.3 ± 0.02	1.0 ± 0.1	7.0 ± 0.3	0.3 ± 0.05
TAPS-NWP	1.6 ± 0.1	6.7 ± 0.0	0.4 ± 0.02	1.0 ± 0.1	7.1 ± 0.2	0.3 ± 0.17
CE-MAPS	1.4 ± 0.1	7.1 ± 0.2	0.3 ± 0.01	1.1 ± 0.5	7.0 ± 1.5	0.3 ± 0.19

To two significant figures, and across both methods of estimation, the Ω on-average equal 1.0 (K^{-1}), 7.0 $(kg\ g^{-1})$, and 0.3 (hPa^{-1}), respectively. The Ω_c averages for TAPS-NWP vary slightly from the CE-NWP and CE-MAPS averaged Ω likely due to the higher temperature and humidity conditions (Eq. [6-8]), while the average TAPS-NWP Ω_f are more similar to the average CE-NWP and CE-MAPS Ω_f. To evaluate whether these discrepancies in values are physically important, each set of mean Ω are combined with the known refractivity, temperature, and pressure gradients from the CE-NWP, TAPS-NWP, and CE-MAPS datasets to estimate humidity gradients via Eq. (5). With the estimated humidity gradients, we apply Eq. (10) to obtain vertical profiles of specific humidity. For example, the mean Ω_f from the CE-NWP dataset are used to compute humidity vertical profiles using refractivity, temperature, and pressure gradients from CE-NWP, TAPS-NWP, CE-MAPS, along with Eq. (5) and (10). An example comparison between true humidity and an estimated humidity profile computed using CE-NWP mean Ω_c and CE-NWP, TAPS-NWP, and CE-MAPS refractivity, temperature, and pressure gradients is shown in fig. 5. Specifically, the example in fig. 5b was computed with a = 1.4 (K^{-1}), b = 7.2 $(kg\ g^{-1})$, and c = 0.3 (hPa^{-1}) for CE-NWP

https://doi.org/10.5194/egusphere-2026-4640
Preprint. Discussion started: 20 November 2026
© Author(s) 2026. CC BY 4.0 License.

295 forecast from 10/10/2015 01:00 UTC at 20.66 km offshore. This comparison (Fig. 5b) has a low RMSE (Ψ = 0.020 g kg^{-1}), which is approximately one percent of the average CASPER-East specific humidity, indicating good agreement.

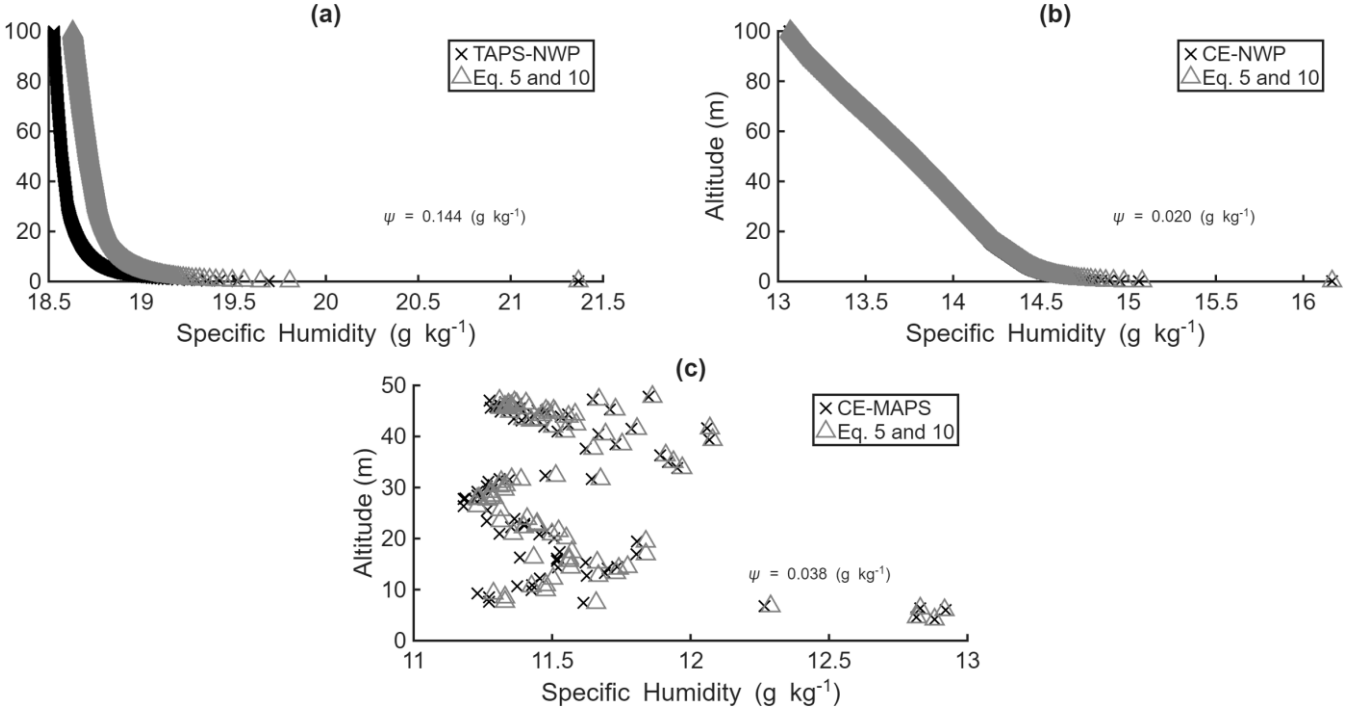


Figure 5. Example vertical profiles of specific humidity from TAPS COAMPS (a), CE COAMPS (b), and CE MAPS (c) (black) 300 **and specific humidity estimated using Eq. (5) with mean Ω_f of a = 1.4 K^{-1}, b = 7.2 kg g^{-1}, and c = 0.3 mb^{-1} (grey). Data shown are for CE-NWP and TAPS-NWP forecast for 10/10/2015 01:00 UTC and 24/11/2013 13:00 UTC, respectively. CE-MAPS measurements were taken on 1/11/2015 at 12:30 UTC.**

When using the Ω_c from the CE-NWP for the CE-NWP gradients (Fig. 5b) the agreement is better than using the CE-
305 NWP Ω_c for the CE-MAPS (Fig. 5c) and TAPS-NWP (Fig. 5a) gradients, as expected . Fig. 6 shows RMSEs (Ψ) between the true specific humidity profiles and those computed using Eq. (5) and Eq. (10) with the average Ω_c from each dataset (Table 1). There is one panel for each dataset, where the coefficients used for all the Ψ calculations are based on mean Ω_c from the various datasets – (a, orange) mean Ω_c based-on TAPS-NWP data, (b, dark-grey) mean Ω_c based-on CE-NWP data and (c, light-grey) mean Ω_c based-on CE-MAPS data. For example, the Ψ in fig. 5a would represent one count in fig. 6a, the Ψ in fig. 5b
310 would represent one count in fig. 6b, and the Ψ in fig. 5c would represent one count in fig. 6c. Thus, in each panel, there is one dataset from which the coefficients were determined while the other two use mean coefficients based-on another dataset to estimate humidity for that dataset, and consequently, typically exhibiting higher RMSEs. Utilizing mean TAPS-NWP

https://doi.org/10.5194/egusphere-2026-4640
Preprint. Discussion started: 20 November 2026
© Author(s) 2026. CC BY 4.0 License.

Ω_c to estimate humidity for TAPS gradients (Fig. 6a, orange) are typically below 0.1 g kg^{-1}. In contrast, the Ψs are higher using the mean Ω_c from both CE-NWP (frequently > 0.5 g kg^{-1}) and CE-MAPS (frequently > 0.4 g kg^{-1}) datasets. CE-MAPS results (Fig. 6c) show limited variability of Ψs regardless of which set of mean coefficients were used, potentially due to the low number of observations or the lack of strong surface gradients in comparison to the (blended) NWP data near the surface. In fig. 6b, when mean CE-MAPS Ω_c are used for estimating CE-NWP humidity profiles, most Ψs are well below 0.2 g kg^{-1}, indicating that the small discrepancies in the mean Ω_c based on the CE-NWP vs MAPS data (Table 1) do not make a significant difference in the estimated humidity profiles. This result also reflects good agreement between CE-NWP and CE-MAPS data. Noticeably higher Ψs are present when using TAPS-NWP mean Ω_c (Fig. 6b), suggesting some dependency of the results on location and/or season. This result implies that if Ω are generated from a dataset from one location and used on a dataset in another location errors will be larger. However, in all cases, the differences are still mostly below the standard error of a radiosonde, ~0.6 g kg^{-1}, at mid-latitudes and, ~1.2 g kg^{-1} at low latitudes (Kotthaus et al., 2023).

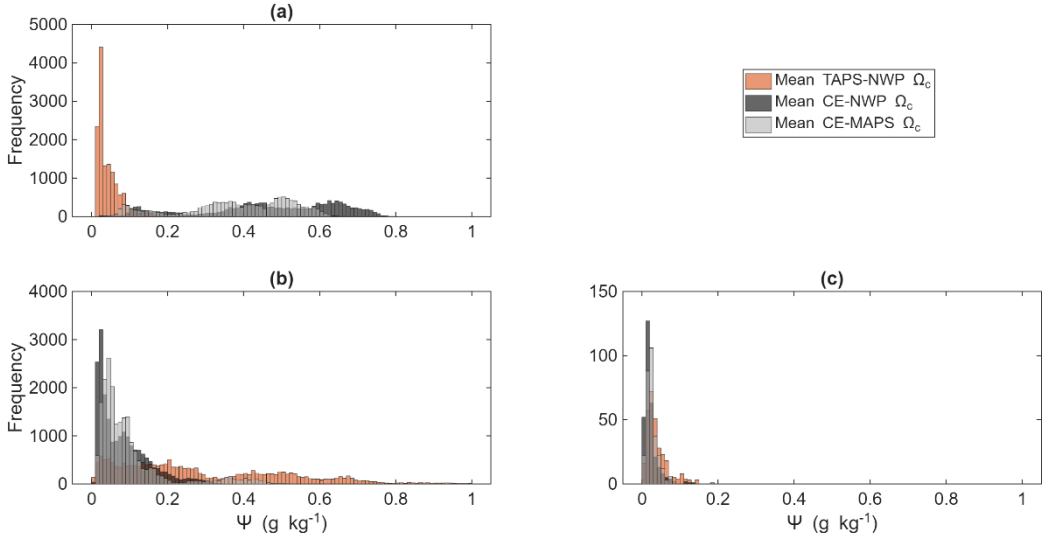


Figure 6. Histograms of RMSEs (Ψs, Eq. (11)) computed between true specific humidities and the estimated specific humidities using Eq. (5) and Eq. (10) along with the mean Ω_c from each dataset (see legend). The different mean Ω_c are shown in Table 1. Results for TAPS-NPW data are shown in (a), CE-NWP in (b), and CE-MAPS data in (c).

Fig. 7 shows the same results as fig. 6 but using mean Ω_f instead of Ω_c. The Ω_f magnitudes for all datasets are within a tenth of a = 1.0 (K^{-1}), b = 7.0 ($kg\,g^{-1}$), and c = 0.3 (hPa^{-1}). The CE-MAPS and CE-NWP Ω_f produce very similar Ψs for their own gradients (Fig. 7b and 7c). In contrast, TAPS Ω_f used with TAPS-NWP (Fig. 7a) commonly has Ψs > 0.6 g kg^{-1}; the largest Ψ for a dataset in which the mean Ω_f were based off the same data. This result suggests high variability in the linear fits for the TAPS-NWP. Fig. 7b and 7c show most Ψs are well below 0.2 g kg^{-1}. The higher RMSEs of the TAPS-NWP,

https://doi.org/10.5194/egusphere-2026-4640
Preprint. Discussion started: 20 November 2026
© Author(s) 2026. CC BY 4.0 License.

regardless of the source of the coefficients (Fig. 7a), indicates that variations in the fit coefficients shown in Table 1 may not adequately capture the variability in the environment at low latitudes. Fig. 7, on average, produces higher RMSEs compared to fig. 6, this result is likely due to the high variability of non-linear fit coefficients. Overall, the RMSEs are small whether used within the same or different data from which the coefficients were derived, suggesting that approximating the coefficients with fixed values would not yield large errors in most cases.

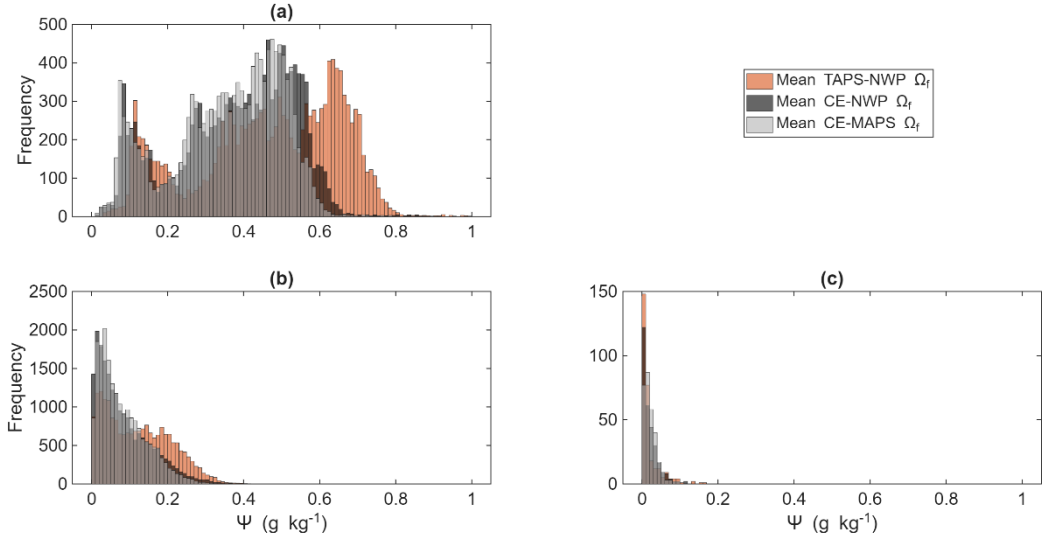


Figure 7. Histograms of RMSEs (Ψs) computed between true specific humidities and the estimated specific humidities using Eq. (5) and Eq. (10) along with the mean Ω_f from each dataset (see legend). The different mean Ω_f are shown in Table 1. TAPS-NWP data are shown in (a), CE-NWP in (b), and CE-MAPS data in (c).

6 Discussion and Conclusions

The derivative of the Bean and Dutton (1966) expression relating refractivity to temperature, pressure, and humidity describes refractivity gradients (Eq. [5]) in the MASL. Following from the techniques described in Gossard et al. (1995) and Stankov et al. (2003) iIn this study, we evaluate the set of coefficients: *a, b*, and *c* (Ω) within this expression, The coefficient sets were estimated using equations originally presented in Gossard et al. (1995) and Stankov et al. (2003) (modified for non-potential variables, Ω_c) as well as those determined from nonlinear least squares fits (Ω_f) of Eq. (5).

It is shown that the vertical profiles of Ω_c and Ω_f are relatively constant in the MASL but vary slightly near the surface (<4 m) where the largest temperature, specific humidity, and atmospheric refractivity gradients exist in the NWP forecasts., The CE-MAPS data does not show this variation likely due to the lowest measurements occurring at ~0.5 m above sea level.

https://doi.org/10.5194/egusphere-2026-4640
Preprint. Discussion started: 20 November 2026
© Author(s) 2026. CC BY 4.0 License.

Collectively, these results suggest that constant coefficients may be applied in Eq. (5); we show that the average *a, b,* and *c* coefficients are 1.0 (K^{-1}), 7.0 $(\mathrm{kg\ g}^{-1})$, and 0.3 (hPa^{-1}), respectively; however, small inter-dataset variations exist.

To assess if these variations are meaningful, humidity and humidity gradients were estimated using constant coefficients derived from one dataset to predict humidity gradients with other datasets' refractivity, pressure, and temperature gradients. When applying the mean coefficients from one dataset with the gradients from another, the RMSE (Ψ) typically increases (Fig. 6 and 7), with the largest $\Psi \approx 1\ \mathrm{g\ kg}^{-1}$ (Fig. 7a). However, this Ψ is within the measurement uncertainty of a radiosonde (Kotthaus et al., 2023) at low-latitudes. Moreover, the mean and median Ψs of all estimated specific humidity profiles over all datasets (~200,000) and coefficient combinations were 0.22 and 0.13 $\mathrm{g\ kg}^{-1}$, respectively. Therefore, while the Ψ is frequently larger when using mean Ω from one dataset to predict another dataset's humidity gradient, the Ψ is still relatively small. Thus, as long as the Ψs equivalent to radiosonde measurement uncertainty is sufficient and altitudes of focus are above 4 m, constant coefficients of a = 1.0 (K^{-1}), b = 7.0 $(\mathrm{kg\ g}^{-1})$, and c = 0.3 (hPa^{-1}) should suffice in application of Eq. (5) in remote sensing applications.

The Gossard et al. (1995) and Stankov et al. (2003) methodologies employed the use of Doppler WRPs to retrieve potential atmospheric refractivity, and theoretically a RASS to retrieve temperature gradients, which could be used to solve for upper atmosphere humidity gradients (Eq. [1]). However, WPRs and RASS are typically unable to obtain MASL measurements and have a very coarse vertical resolution (commonly > 100 m). Developments over the past twenty-five years have yielded methods to estimate refractivity from point-to-point radar wave propagation or sea clutter measurements via RF inversions. These RF inversion methods may be used in conjunction with Eq. (5) and (10) and a surface layer temperature profile from NWP or another sensor (NWP has been shown to predict temperature more accurately than moisture, Sease 2024), and constant coefficients described herein, to retrieve humidity vertical profiles in the MASL. Such remote sensing of the water vapor structure of the MASL can be used to better inform weather prediction forecasts, improve surface layer modelling, and provide more accurate environmental characterization for propagation predictions for RF, laser, acoustic, and communication signals.

Appendix A

This study investigates the extension of a ground based tropospheric humidity remote sensing methodology to the MASL. We have shown that surface layer humidity can be accurately resolved using the aforementioned methodology, however, we did not present the converse scenario of estimating temperature gradients with known or measured humidity gradients. Therefore, here we estimate temperature from known refractivity, specific humidity, and pressure gradients along with Eq. (5), using constant coefficients to see if similar trends in the coefficients are observed when solving for temperature rather than humidity:

https://doi.org/10.5194/egusphere-2026-4640
Preprint. Discussion started: 20 November 2026
© Author(s) 2026. CC BY 4.0 License.

$$\frac{d\tilde{T}}{dz} = a^{-1}\left(b\frac{dq}{dz} - \frac{dN}{dz} + c\frac{dp}{dz}\right) \quad \text{(A1)}$$

$$\tilde{T}(z_i) = \tilde{T}(z_{i-1}) + \frac{d\tilde{T}}{dz}(z_{i-1})\Delta z \quad \text{(A2)}$$

We apply the same methods as presented in fig. 6 and 7 for fig. 8 and 9 with Eq. (A1) and (A2) instead of Eq. (5) and (10). These figures show RMSEs between the true temperature and estimated temperature when constant Ω from each dataset are applied to the (a) TAPS-NWP, (b) CE-NWP, (c) and CE-MAPS gradients. We find that RMSEs are significantly higher when solving for temperature instead of specific humidity, relative to the accuracy of modern humidity and temperature sensors (Kotthaus et al., 2023; Bianco et al., 2024).

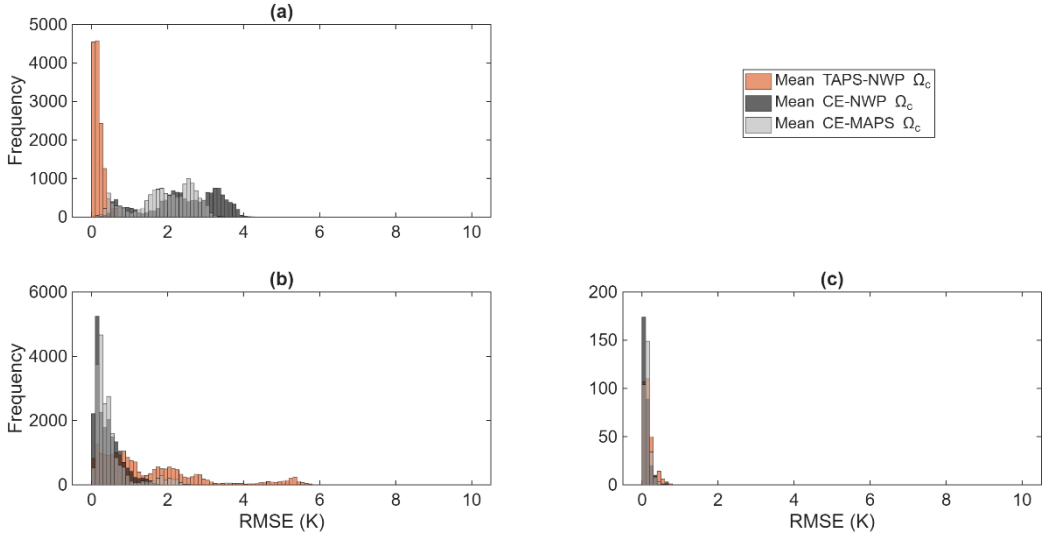


Figure A1: Histograms of RMSEs (Ψ) computed between true temperatures and the estimated temperatures using Eq. (A1) and Eq. (A2) along with the mean Ω_c from each dataset. Different colors represent the different mean Ω_c shown in Table 1 (see legend). TAPS-NPW data is shown in (a), CE-NWP in (b), and CE-MAPS data in (c).

Similarly to fig. 6, fig. 8 shows that the mean Ω_c for each dataset produces the lowest RMSEs (Ψs) when using their respective gradients. For example, in fig. 8a the TAPS-NWP mean Ω_c produces $\Psi < 1$ K while the CE-MAPS and CE- NWP Ω_c produce RMSEs between 2 and 4 K. A similar result is shown in fig. 8b but to a lesser degree. However, in the CE-MAPS dataset we observe $\Psi < 1$ K for all mean Ω_c, once again, plausably due to the low number of observations or lack of large surface gradients. We find that temperatures estimated via Eq. (A1) are more sensitive to small changes in coefficient values relative to humidity (Eq. [5]). Average Ω_f for the three datasets only differ by a tenth but those differences can cause a several

https://doi.org/10.5194/egusphere-2026-4640
Preprint. Discussion started: 20 November 2026
© Author(s) 2026. CC BY 4.0 License.

degree difference in the temperature RMSEs. Thus, constant coefficients are recommended primarily for estimating humidity rather than temperature, which could be sensitive to small variations in coefficient values.

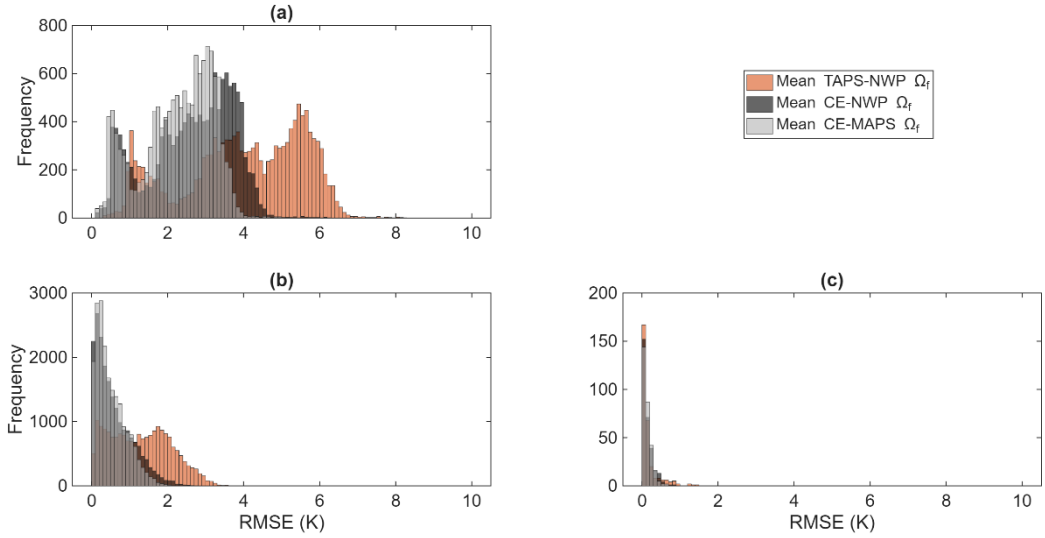


Figure A2: Histograms of RMSEs (Ψ) computed between true temperatures and the estimated temperatures using Eq. (A1) and Eq. (A2) along with the mean Ω_f from each dataset. Different colors represent the different mean Ω_f shown in Table 1 (see legend). TAPS-NPW data is shown in (a), CE-NWP in (b), and CE-MAPS data in (c).

Code, data, or code and data availability

Data shown in the figures are available from the corresponding author upon request.

Supplement link

The link to the supplement will be included by Copernicus, if applicable.

Author contributions

Conceptualization, E.E.H.; methodology, D.P.G., E.E.H. and C.R.S.; formal analysis, C.R.S.; investigation, D.P.G., E.E.H. and C.R.S.; data curation, A.J.K and D.D.F.; writing—original draft preparation, C.R.S.; writing—review and editing, D.P.G., A.J.K,

https://doi.org/10.5194/egusphere-2026-4640
Preprint. Discussion started: 20 November 2026
© Author(s) 2026. CC BY 4.0 License.

415 D.D.F, E.E.H. and C.R.S.; supervision, E.E.H.; project administration, E.E.H.; funding acquisition, E.E.H. All authors have read and agreed to the published version of the manuscript.

Competing interests

The authors declare that they have no conflict of interest.

Disclaimer

420 Copernicus Publications adds a standard disclaimer: "Copernicus Publications remains neutral with regard to jurisdictional claims made in the text, published maps, institutional affiliations, or any other geographical representation in this paper. While Copernicus Publications makes every effort to include appropriate place names, the final responsibility lies with the authors. Views expressed in the text are those of the authors and do not necessarily reflect the views of the publisher." Please feel free to add disclaimer text at your choice, if applicable.

425 **Acknowledgements**

The authors would like to thank Qing Wang and Ryan Yamaguchi at the Naval Postgraduate School for the CASPER-East *in-situ* data and Madison Bruno for initial research. AI assistance was used for preparation of the reference list, initial drafts of code, and editorial recommendations on the text.

Financial support

430 This research was funded by the Office of Naval Research (N00014-23-C-2033).

Review statement

The review statement will be added by Copernicus Publications listing the handling editor as well as all contributing referees according to their status anonymous or identified.

References

435 Bean, B. R. and Dutton, E. J.: *Radio meteorology*, 1st edn., College Entrance Book Company, New York, USA, 1966.

https://doi.org/10.5194/egusphere-2026-4640
Preprint. Discussion started: 20 November 2026
© Author(s) 2026. CC BY 4.0 License.

Bianco, L., Adler, B., Bariteau, L., Djalalova, I. V., Myers, T., Pezoa, S., Turner, D. D., and Wilczak, J. M.: Sensitivity of thermodynamic profiles retrieved from ground-based microwave and infrared observations to additional input data from active remote sensing instruments and numerical weather prediction models, *Atmos. Meas. Tech.*, 17, 3933–3948, https://doi.org/10.5194/amt-17-3933-2024, 2024.

Calaf, M., Vercauteren, N., Katul, G. G., et al.: Boundary-layer processes hindering contemporary numerical weather prediction models, *Bound.-Lay. Meteorol.*, 186, 43–68, https://doi.org/10.1007/s10546-022-00742-5, 2023.

Che, Y., Ma, S., Xing, F., et al.: An improvement of the retrieval of temperature and relative humidity profiles from a combination of active and passive remote sensing, *Meteorol. Atmos. Phys.*, 131, 681–695, https://doi.org/10.1007/s00703-018-0588-3, 2019.

Edson, J. B. and Fairall, C. W.: Similarity relationships in the marine atmospheric surface layer for terms in the turbulent kinetic energy and scalar variance budgets, *J. Atmos. Sci.*, 55, 2311–2328, https://doi.org/10.1175/1520-0469(1998)055<2311:SRITMA>2.0.CO;2 , 1998.

Frederickson, P. A.: Further improvements and validation for the Navy Atmospheric Vertical Surface Layer Model (NAVSLaM), in: *Proceedings of the USNC–URSI Radio Science Meeting*, Vancouver, BC, Canada, 242, https://doi.org/10.1109/USNC-URSI.2015.7303526, 2015.

Gerstoft, P., Rogers, L. T., Wagner, L. J., and Hodgkiss, W. S.: Estimation of radio refractivity structure using radar clutter, in: *Proceedings of the MTS/IEEE OCEANS 2001 Conference*, Honolulu, HI, USA, 636–641, https://doi.org/10.1109/OCEANS.2001.968797, 2001.

Gerstoft, P., Rogers, L. T., Krolik, J. L., and Hodgkiss, W. S.: Inversion for refractivity parameters from radar sea clutter, *Radio Sci.*, 38, https://doi.org/10.1029/2002RS002640, 2003.

Gossard, E. E., Strauch, R. G., Stankov, B. B., and Wolfe, D. E.: Measurement of property gradients and turbulence aloft with ground-based Doppler radars, *J. Atmos. Ocean. Technol.*, 12, 105–123, 1995.

Greenway, D. P. and Hackett, E. E.: Laterally heterogeneous refractivity inversions using simulated and measured X-band radar data during evaporation ducting conditions, in: *Proceedings of the IEEE INC–USNC–URSI Radio Science Meeting*, Florence, Italy, 270, https://doi.org/10.23919/INC-USNC-URSI61303.2024.10632225, 2024.

Hodur, R. M.: The Naval Research Laboratory's coupled ocean–atmosphere mesoscale prediction system (COAMPS), *Mon. Weather Rev.*, 125, 1414–1430, https://doi.org/10.1175/1520-0493(1997)125<1414:TNRLCO>2.0.CO;2, 1997.

Jason A. Otkin, Daniel C. Hartung, Daniel D. Turner, Ronald A. Petersen, William F. Feltz, and Edward Janzon: Assimilation of surface-based boundary layer profiler observations during a cool-season weather event using an observing system simulation experiment. Part I: Analysis impact, *Mon. Weather Rev.*, 139, 2309–2326, https://doi.org/10.1175/2011MWR3622.1, 2011.

Kammerer, A. J., Haack, T., Norris, R., Hansen, H., Kulessa, A., and Barrios, A.: Predicting RF propagation with numerical models, *Proc. IEEE Int. Symp. on Antennas and Propagation & USNC/URSI National Radio Science Meeting*, Boston, MA, USA, 1927–1928, https://doi.org/10.1109/APUSNCURSINRSM.2018.8609197, 2018.

https://doi.org/10.5194/egusphere-2026-4640
Preprint. Discussion started: 20 November 2026
© Author(s) 2026. CC BY 4.0 License.

Kang, D. and Wang, Q.: Optimized estimation of surface layer characteristics from profiling measurements, *Atmosphere*, 7, 14, https://doi.org/10.3390/atmos7020014, 2016.

Karimian, A., Yardim, C., Gerstoft, P., Hodgkiss, W. S., and Barrios, A. E.: Refractivity estimation from sea clutter: An invited review, *Radio Sci.*, 46, RS6001, https://doi.org/10.1029/2011RS004818, 2011.

Karimian, A., Yardim, C., Hodgkiss, W. S., Gerstoft, P., and Barrios, A. E.: Estimation of radio refractivity using a multiple-angle clutter model, *Radio Sci.*, 47, RS3002, https://doi.org/10.1029/2011RS004701, 2012.

Karimian, A., Yardim, C., Haack, T., Gerstoft, P., Hodgkiss, W. S., and Rogers, T.: Toward the assimilation of the atmospheric surface layer using numerical weather prediction and radar clutter observations, *J. Appl. Meteorol. Climatol.*, 52, 2345–2355, https://doi.org/10.1175/JAMC-D-12-0320.1, 2013.

Kotthaus, S., Bravo-Aranda, J. A., Collaud Coen, M., Guerrero-Rascado, J. L., Costa, M. J., Cimini, D., et al.: Atmospheric boundary layer height from ground-based remote sensing: A review of capabilities and limitations, *Atmos. Meas. Tech.*, 16(2), 433-479, https://doi.org/10.5194/amt-16-433-2023, 2023.

Kulessa, A. S., Barrios, A., Claverie, J., Garrett, S., Haack, T., Hacker, J. M., et al.: The Tropical Air–Sea Propagation Study (TAPS), *Bull. Am. Meteorol. Soc.*, 98, 517–537, https://doi.org/10.1175/BAMS-D-14-00284.1, 2017.

Matsko, I. J. and Hackett, E. E.: Impact of radar data sampling on the accuracy of atmospheric refractivity inversions over marine surfaces, *Radio Sci.*, 54, 704–714, https://doi.org/10.1029/2018RS006757, 2019.

Monin, A. S. and Obukhov, A. M.: Basic laws of turbulent mixing in the surface layer of the atmosphere, *Tr. Geofiz. Inst. Akad. Nauk SSSR*, 151, 163–187, 1954.

Pastore, D. M., Greenway, D. P., Stanek, M. J., Wessinger, S. E., Haack, T., Wang, Q., and Hackett, E. E.: Comparison of atmospheric refractivity estimation methods and their influence on radar propagation predictions, *Radio Sci.*, 56, e2020RS007244, https://doi.org/10.1029/2020RS007244, 2021.

Pastore, D. M., Yamaguchi, R. T., Wang, Q., and Hackett, E. E.: On the variability of in situ surface layer refractivity measurements, *Atmosphere*, 14, 1085, https://doi.org/10.3390/atmos14071085, 2023.

Pastore, D. M., Wessinger, S. E., Greenway, D. P., Stanek, M. J., Burkholder, R. J., Haack, T., et al.: Refractivity inversions from point-to-point X-band radar propagation measurements, *Radio Sci.*, 57, e2021RS007345, https://doi.org/10.1029/2021RS007345, 2022.

Rogers, L. T., Hattan, C. P., and Stapleton, J. K.: Estimating evaporation duct heights from radar sea echo, *Radio Sci.*, 35, 955–966, https://doi.org/10.1029/1999RS002275, 2000.

Rogers, L. T., Jablecki, M., and Gerstoft, P.: Posterior distributions of a statistic of propagation loss inferred from radar sea clutter, *Radio Sci.*, 40, https://doi.org/10.1029/2004RS003112, 2005.

https://doi.org/10.5194/egusphere-2026-4640
Preprint. Discussion started: 20 November 2026
© Author(s) 2026. CC BY 4.0 License.

Ruggiero, F. H., Sashegyi, K. D., Madala, R. V., and Raman, S.: The use of surface observations in four-dimensional data assimilation using a mesoscale model, *Mon. Weather Rev.*, 124, 1018–1033, https://doi.org/10.1175/1520-0493(1996)124<1018:TUOSOI>2.0.CO;2, 1996.

Sease, C. R.: Error Analysis of Numerical Weather Prediction Forecasts and Remotely Sensed Air Properties, Undergraduate Honors Thesis, Coastal Carolina University, Conway, SC, USA, 2024.

Stanek, M. J.: Ocean wave-coherent temperature and humidity near-surface vertical distributions and their effect on radar performance over the ocean, PhD thesis, Coastal Carolina University, Conway, SC, USA, 2023.

Stanek, M. J., Pastore, D. M., and Hackett, E. E.: A novel near-surface wave-coherent instantaneous profiling system for atmospheric measurements, *Sensors*, 23, 4099, https://doi.org/10.3390/s23084099, 2023.

Stankov, B. B., Gossard, E. E., Weber, B. L., Lataitis, R. J., White, A. B., Wolfe, D. E., Welsh, D. C., and Strauch, R. G.: Humidity gradient profiles from wind profiling radars using the NOAA/ETL advanced signal processing system, *J. Atmos. Ocean. Technol.*, 20, 3–22, https://doi.org/10.1175/1520-0426(2003)020<0003:HGPFWP>2.0.CO;2, 2003.

Ulate, M., Wang, Q., Haack, T., Holt, T., and Alappattu, D. P.: Mean offshore refractive conditions during the CASPER East field campaign, *J. Appl. Meteorol. Climatol.*, 58, 853–874, https://doi.org/10.1175/JAMC-D-18-0029.1, 2019.

Wang, Q., Alappattu, D. P., Billingsley, S., Blomquist, B., Burkholder, R. J., Christman, A. J., and Franklin, K. B.: CASPER: Coupled air–sea processes and electromagnetic ducting research, *Bull. Am. Meteorol. Soc.*, 99, 1449–1471, https://doi.org/10.1175/BAMS-D-16-0046.1, 2018.

Wang, Q., et al.: Radar and electromagnetic ducting in stable atmosphere over water (REDSAW), in: *Proceedings of the USNC–URSI National Radio Science Meeting*, Boulder, CO, USA, 48, https://doi.org/10.23919/USNC-URSINRSM60317.2024.10464746, 2024.

Wessinger, S. E., Greenway, D. P., Haack, T., and Hackett, E. E.: Near-surface thermodynamic influences on evaporation duct shape, *Atmosphere*, 15, 718, https://doi.org/10.3390/atmos15060718, 2024.

Xu, L., Yardim, C., and Haack, T.: Evaluation of COAMPS boundary layer refractivity forecast accuracy for 2–40 GHz electromagnetic wave propagation, *Radio Sci.*, 57, e2021RS007404, https://doi.org/10.1029/2021RS007404, 2022.

Yardim, C., Gerstoft, P., and Hodgkiss, W. S.: Estimation of radio refractivity from radar clutter using Bayesian Monte Carlo analysis, *IEEE Trans. Antennas Propag.*, 54, 1318–1327, https://doi.org/10.1109/TAP.2006.872673, 2006.

Yardim, C., Gerstoft, P., and Hodgkiss, W. S.: Tracking refractivity from clutter using Kalman and particle filters, *IEEE Trans. Antennas Propag.*, 56, 1058–1070, https://doi.org/10.1109/TAP.2008.919205, 2008.

Yardim, C., Gerstoft, P., and Hodgkiss, W. S.: Sensitivity analysis and performance estimation of refractivity-from-clutter techniques, *Radio Sci.*, 44, RS1001, https://doi.org/10.1029/2008RS003897, 2009.

Zhao, X., Huang, S., and Du, H.: Theoretical analysis and numerical experiments of variational adjoint approach for refractivity estimation, *Radio Sci.*, 46, RS1006, https://doi.org/10.1029/2010RS004417, 2011.

https://doi.org/10.5194/egusphere-2026-4640
Preprint. Discussion started: 20 November 2026
© Author(s) 2026. CC BY 4.0 License.



Zhao, X., Yardim, C., Wang, D., and Howe, B. M.: Estimating range-dependent evaporation duct height, *J. Atmos. Ocean. Technol.*, 34, 1113–1123, https://doi.org/10.1175/JTECH-D-16-0125.1, 2017.